JOURNAL OF THE ROYAL SOCIETY Interface

Correlating cell morphology and osteoid mineralization relative to strain profile for bone tissue engineering applications

M.A Wood, Y Yang, E Baas, D.O Meredith, R.G Richards, J.H Kuiper and A.J El Haj

J. R. Soc. Interface 2008 **5**, 899-907
doi: 10.1098/rsif.2007.1265

JOURNAL OF THE ROYAL SOCIETY Interface

J. R. Soc. Interface (2008) **5**, 899–907
doi:10.1098/rsif.2007.1265
Published online 11 December 2007

Correlating cell morphology and osteoid mineralization relative to strain profile for bone tissue engineering applications

M. A. Wood[1,*], Y. Yang[1], E. Baas[1], D. O. Meredith[2], R. G. Richards[2], J. H. Kuiper[1] and A. J. El Haj[1]

[1]*Institute of Science and Technology in Medicine, Keele University, Thornburrow Drive, Hartshill, Staffordshire ST4 7QB, UK*
[2]*AO Research Institute, AO Foundation, Clavadelerstrasse 8, 7270 Davos Platz, Switzerland*

A number of bone tissue engineering strategies use porous three-dimensional scaffolds in combination with bioreactor regimes. The ability to understand cell behaviour relative to strain profile will allow for the effects of mechanical conditioning in bone tissue engineering to be realized and optimized. We have designed a model system to investigate the effects of strain profile on bone cell behaviour. This simplified model has been designed with a view to providing insight into the types of strain distribution occurring across a single pore of a scaffold subjected to perfusion–compression conditioning. Local strains were calculated at the surface of the pore model using finite-element analysis. Scanning electron microscopy was used in secondary electron mode to identify cell morphology within the pore relative to local strains, while backscattered electron detection in combination with X-ray microanalysis was used to identify calcium deposition. Morphology was altered according to the level of strain experienced by bone cells, where cells subjected to compressive strains (up to 0.61%) appeared extremely rounded while those experiencing zero and tensile strain (up to 0.81%) were well spread. Osteoid mineralization was similarly shown to be dose dependent with respect to substrate strain within the pore model, with the highest level of calcium deposition identified in the intermediate zones of tension/compression.

Keywords: cell morphology; biomineralization; calcium; bone tissue engineering; strain profile; finite-element analysis

1. INTRODUCTION

Mechanical compression resulting in mechanotransduction, the process whereby mechanical signals are converted into a series of biochemical signalling events (Nomura & Takano-Yamamoto 2000), is known to enhance bone formation both *in vitro* (Mullender *et al.* 2004) and *in vivo* (Turner & Robling 2004). Although a common mechanism is believed to underlie this phenomenon regardless of cell type (Iqbal & Zaidi 2004), the finer points of the process require to be elucidated. For example, mechanical compression has been shown to enhance calcium levels in tissue-engineered bone constructs (Wood *et al.* 2006*b*), yet little is known regarding temporal and spatial mineral deposition occurring as a direct result of load profile in a porous three-dimensional system similar to scaffolds used for bone tissue engineering applications. The ability to establish a relationship between these factors, if any exists, would allow the development of load-bearing tissue-engineered constructs with greater functionality, improved loading regimes for *in vitro* and *in vivo* applications and an enhanced understanding of many pathological problems observed in orthopaedic research.

In recent years, tissue engineering has emerged as a promising therapy for the treatment of tissue or organ damage or loss in orthopaedics (Oakes 2004). The main routes to producing tissue-engineered bone incorporate three basic elements, namely cells, growth factors and three-dimensional polymeric scaffolds (Hing 2004). Cell-seeded constructs are generally cultured in bioreactors, for example spinner flasks and rotating wall vessel reactors, to increase diffusion throughout the system and in an attempt to mimic the dynamics of *in vivo* conditions, where mechanical stimulation, in the form of hydrostatic pressure and shear stress, is experienced by cells and tissues (Salgado *et al.* 2004). Regardless of the approach taken, the mechanical properties of the scaffolds must be considered if the final construct is to be used clinically due to the continuous strain experienced in the bone environment *in vivo* (Turner & Robling 2004).

*Author and address for correspondence: Centre for Cell Engineering, Division of Infection and Immunity, Joseph Black Building, University of Glasgow, Glasgow G12 8QQ, UK (m.wood@bio.gla.ac.uk).

Received 12 October 2007
Accepted 17 November 2007

With developments in bioreactor manufacture (El Haj *et al.* 2005) and scaffold design (Sikavitsas *et al.* 2001), mechanical conditioning of constructs, mimicking *in vivo* physiological environments for load-bearing tissues, is emerging as an alternative method of optimizing tissue formation *in vitro* (Ignatius *et al.* 2005). Moreover, techniques are being developed which further enhance load effects provided by a perfusion–compression bioreactor system. For example, the dihydropyridine agonist Bay K8644 has been encapsulated and released from mechanically robust scaffolds, acting to augment the opening state of L-type voltage-operated calcium channels (VOCC) following their activation via a controlled loading regime (Yang *et al.* 2002). The effects of Bay K8644-encapsulated scaffolds on bone tissue formation in the presence of load include increased collagen I production and osteoid mineralization within constructs (Wood *et al.* 2006*b*). Thus, mechanical conditioning of cell-seeded constructs, often in the presence of biochemicals, is attracting a great deal of attention due to reports of accelerated tissue production in three-dimensional scaffolds and matrices.

However, even if constructs are subjected to a constant level of load, cells will perceive different local strains due to the irregular distribution of pores within the scaffold. How the spatial strain distribution affects cell morphology and mineralization, in the case of engineered bone, has yet to be fully deduced. We have developed a simple *in vitro* model allowing for the spatial effects of strain to be investigated relative to applied load. In this instance, the strain experienced by cells within the model is applied using a perfusion–compression bioreactor as observed during the mechanical conditioning of constructs for bone tissue engineering applications.

2. MATERIALS AND METHODS

2.1. Pore model

A model pore was produced using medical-grade silicone tubing (internal ϕ2 mm, external ϕ3 mm and length 5 mm). The tubing was briefly etched in diluted chromic acid for 3 s to roughen the inner surface of the construct, followed by rinsing in copious amounts of water. The inner surface of the tubing was then coated with collagen type 1 from calf skin in an acetic acid solution (Sigma) prior to cell seeding, to encourage cell attachment. Excess acetic acid was removed by thoroughly rinsing the tube with phosphate-buffered saline.

2.2. Cell culture

Bone cells were grown from rat tibia bone chips, as outlined elsewhere (Walker *et al.* 2000) and cultured in Dulbecco's modified Eagles medium supplemented with 10% foetal calf serum, 2 mM L-glutamine, 25 nM ascorbic acid, 100 nM dexamethasone, 10 mM β-glycerophosphate and 1% (v/v) antibiotic and antimycotic solution (Sigma). Media was supplemented with 1 µM Bay K8644, a calcium channel agonist known to enhance bone production in three-dimensional constructs subjected to mechanical conditioning in a perfusion–compression bioreactor (Wood *et al.* 2006*a*,*b*). Approximately 3×10^6 cells ml^{-1} solution was used to fill the silicone tubing at passage 1. The cell-seeded constructs were placed with the longitudinal axis horizontal and cultured statically for 3 days, following which samples were separated into two groups where cell-seeded tubes were subjected to a further 3 days of either (i) control, static (n=6) or (ii) perfusion–compression (n=6) conditioning. Static conditioning refers to the absence of mechanical conditioning, where samples are placed in a Petri dish in an incubator only.

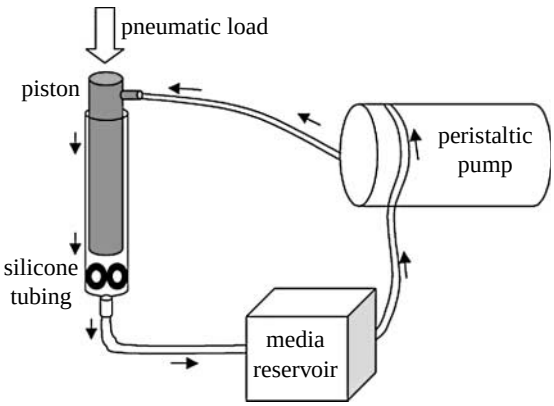

Figure 1. A schematic of one circuit of the perfusion–compression bioreactor used to provide load to the pore model. Media is placed within the reservoir and is circulated to the construct via tubing in combination with a peristaltic pump. The metal piston has a hollow bore with five small holes at the lower end, allowing media to flow to the silicone tubing unabated. The media then completes the circuit upon returning to the reservoir. Compression is applied to the head of the piston via a pneumatic regime, which is transferred to the cells contained within the inner surface of the single pore model. The arrows indicate the direction of media flow.

2.3. Bioreactor conditioning

Mechanical conditioning was induced via a perfusion–compression bioreactor where constructs were subjected to cyclic load for 1 h d^{-1} at 37°C at a frequency of 1 Hz, during the 3-day conditioning phase. A pneumatic system was used to provide compressive pressure. Under these conditions, the displacement level was calculated at approximately 1% of the external diameter of the construct using a long focal length microscope, where the displacement of the material under load (alterations in the dimensions of the scaffold) was measured from these images and converted to a percentage relative to the height of the scaffold prior to loading (Wood *et al.* 2006*b*). The bioreactor, equipped with six reservoirs, provided media to each tubing sample within each circuit, where 20 ml media was supplied to the samples during the conditioning period. Perfusion was achieved using a Watson–Marlow snap-fit cassette system and peristaltic pump with perfusion rate set at 0.1 ml min^{-1}. A schematic overview of the bioreactor is presented in figure 1. Control samples were left under static conditions (i.e. tubing samples were placed in a Petri dish in an incubator in the absence of mechanical conditioning).

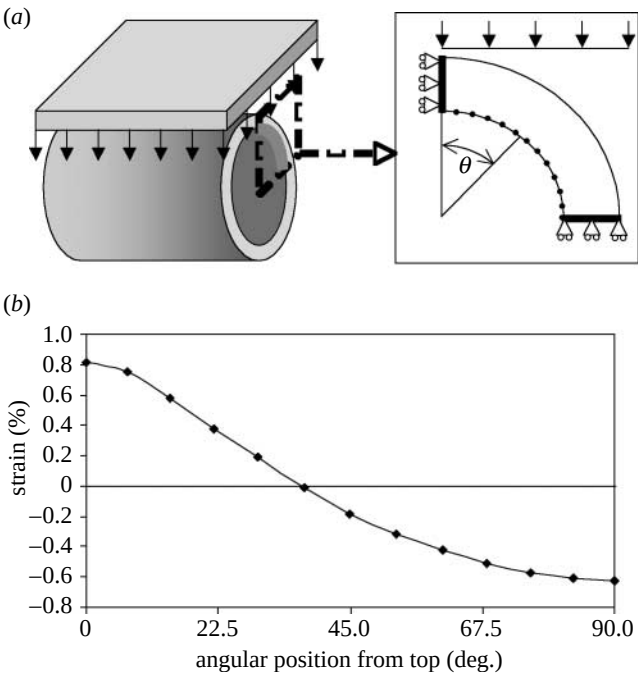

Figure 2. (*a*) A FE model of the silicone tubing was used to estimate the surface strain inside the construct when 1% compression was applied. Owing to the symmetry of the tubing, only one quarter was modelled. (*b*) The positive values in the graph correspond to tension while the negative values indicate compression.

2.4. Modelling of strain distribution

The surface strain inside the single pore model due to a deformation of 1% of the external diameter was estimated using a finite-element (FE) model, which was generated and analysed using MSC.Marc/Mentat, MSC Software. Owing to the symmetry of the pore, the strain values in only one quarter of the construct were examined (figure 2*a*). The pore was modelled using 12 eight-node hybrid plain strain elements (MSC.Marc element type 32). The elastic deformation of the material was modelled with a Mooney–Rivlin model based on data for a medical-grade silicone rubber (MED4950, NuSil Technology LLC, Sophia Antipolis, France: c10 = 0.513 MPa, c01 = 0.013 MPa, bulk modulus k = 65 MPa). The 1% deformation was applied using contact elements (figure 2). The strain at the inner surface, parallel to the surface in circumferential direction of the cylinder, was calculated in 13 points (six adjacent elements, each with three nodes at the inner surface; figure 2*a*).

2.5. SEM preparation

Following conditioning of cells within the single pore model, samples were prefixed in 4% formaldehyde in 0.1 M piperazine-1,4-bis-2-ethane sulphonic acid (PIPES, Fluka), pH 7.2. Prefixed samples were rinsed in PIPES and fixed for 15 min in 2.5% glutaraldehyde in PIPES, subsequently washed in double distilled water and dehydrated in an ethanol series, followed by three rinses in 100% Fluorosil (1,1,2-trichloro-1,2,2-trifluoroethane), the transition fluid, at 5 min intervals. Specimens were then critically point dried in a POLARON E3000 critical point drier prior to sectioning single pore models into quarters. This involved cutting the pore into sections ensuring that the areas under investigation were a true representation of the strain profile being examined. Samples were subsequently mounted on aluminium stubs and coated with 10 nm carbon using a Baltec CED030 carbon thread evaporation unit (Balzers, Liechtenstein). A rotating stage was used when coating samples to ensure even coating of the concave surface.

2.6. Secondary electron and backscattered electron imaging and X-ray microanalysis of samples

Backscattered electron (BSE) detection in combination with X-ray microanalysis allows for mineralized tissue to be identified relative to its location within the pore model. Briefly, BSEs are related to the atomic number of the material (Z) from which they are emitted, providing information regarding the specimen density (Palluel 1947). With respect to osteoid mineralization, calcium is a medium-density material (Z = 20) in a field of low-density organic matter, namely cells and matrix. Thus the two materials can be identified relative to one another within a specimen by providing variation in the number of BSEs produced, affecting image contrast (Wood *et al.* 2005). X-ray microanalysis can then be employed to identify the elemental composition of the bright, dense regions allowing for a positive identification to be made with respect to mineralized osteoid. An X-ray detector fitted within an FESEM with BSE detector permits these techniques to run concurrently (Wood *et al.* 2002). For this work, a Hitachi S-4100 FESEM equipped with an Autrata-modified yttrium aluminium garnet single crystal scintillation BSE detector (Institute of Scientific Instrumentation, Prague, Czech Republic) was used to image samples. The largest condenser aperture measuring 100 µm was used, maximizing the number of electrons in the primary beam, increasing BSE production following interaction of the beam with the specimen. The maximum condenser lens current (C18 setting) was also used, further optimizing the resolution of the FESEM by minimizing the spot size of the primary beam preventing spreading of primary electrons within the specimen. The Hitachi S-4100 was operated using an acceleration voltage of 5 keV. In secondary electron (SE) mode an emission current of 10 µA was used, while in BSE mode 50 µA emission current was selected. A working distance of 10 mm was used under these conditions, optimizing BSE collection and resultant resolution. EDX (Isis 300, Oxford Instruments, Whitney, UK) was performed at 20 keV accelerating voltage.

2.7. Calculating calcium distribution relative to strain profile

BSE mode was used to detect dense materials in one quadrant of the pore model. Two areas within the quadrant, measuring 120×90 µm, were identified as

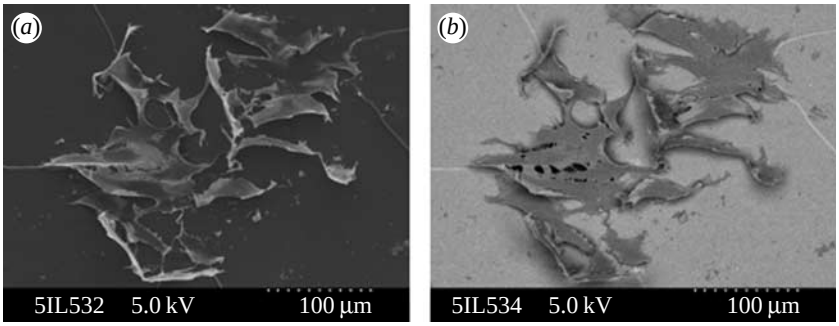

Figure 3. Bone cells cultured under static conditions exhibited flat, well-spread morphology, as seen in (*a*) SE mode regardless of positioning within the tube. (*b*) When imaged in BSE mode, medium- and high-density entities were absent.

containing dense material. Six samples of the dense material identified within these regions were then investigated for their elemental composition using EDX. The results are presented in a scatter plot with data points connected by smooth lines.

3. RESULTS

3.1. FE analysis of strain distribution within the single pore model

The surface strain of the inner surface of the pore was modelled using FE analysis (figure 2). The positive values in the graph correspond to tension while the negative values indicate compression of the material in the FE model (figure 2*b*). The results indicate that a 0.82% tensile strain is generated at the top and bottom of the tubing (0° and 180°). At the right and left sides of the tubing (90°and 270°), a 0.61% compressive strain is generated. These results were virtually insensitive to the exact material properties: a 10-fold variation in the elastic properties gave maximum strain variations below 10^{-6} (1 µstrain). Moving from the top or bottom to a side location results in the tensile strain decreasing until reaching zero almost halfway across this region, before becoming increasingly compressive towards the side of the cylinder, and vice versa.

3.2. Bone cell morphology in static controls

Cells cultured under static conditions exhibited flat, well-spread morphologies as observed in images taken in SE mode (figure 3*a*). When imaged in BSE mode, there was a distinct lack of medium- and high-density material, indicating that bone cells cultured under these conditions were not capable of biomineralization.

3.3. Bone cell morphology as a result of strain distribution

Mechanically conditioned bone cells were imaged relative to their location within the pore model (figure 4). Cells located within a very narrow region at the top and bottom of the tubing were flat and well spread (figure 4(i)), indicating the effects of the surface tensile strain on cell morphology in this area. There was also an absence of mineralization within this region. These results are similar to those observed in static controls (figure 3) suggesting that tensile strain in this region is not as predicted in the FE model, but more similar to static conditions. A lesser amount of strain is observed in the FE model between the vertical and horizontal locations due to the transition from tension to compression as a result of strain dissipation throughout the pore (figure 2). Cells located within these regions tended to form multicellular aggregates containing a number of dense agglomerates identified as bright entities in the BSE images (figure 4(ii)). These were investigated at higher magnification using BSE in combination with EDX (figures 5–7). Cells within a thin region at the side of the tubing, believed to be subjected to the highest levels of compression, appeared extremely rounded (figure 4(iii)) and did not contain dense material.

3.4. Identification of calcium using BSE detection and EDX at low magnification

Dense features, appearing as bright entities in BSE images, were absent in static controls and observed only in regions of the pore model subjected to a reduction in surface strain levels relative to the areas of the model experiencing maximum tension and maximum compression (figure 4(ii)). Following identification of these features at low magnification, EDX was employed to investigate their chemical composition (figures 5 and 6). Not all dense features contained calcium, region 1 and spectrum 1 in figures 5*a* and 6, respectively; however, many of these entities were observed to contain calcium with a peak prevalent at 3.7 keV identified using EDX, regions 2–4 and spectra 2–4 in figures 5*a* and 6, respectively. Identification of calcium-containing material at low magnification (figures 4*b* and 5*a*) allowed for an overall view of the calcium distribution to be identified prior to more precise investigation at higher magnification using BSE detection (figure 7). All silicone peaks in the EDX graphs are believed to originate from the pore model material, while all peaks observed at the left of the graphs occur due to background, including sample coating and organic material in the form of carbon, nitrogen and oxygen components. It should be noted that light elements including carbon, nitrogen and oxygen compose the organic fraction of bone, including cells and osteoid, and also constitute a portion of the mineral phase (Vajda *et al.* 1996) with oxygen comprising a large

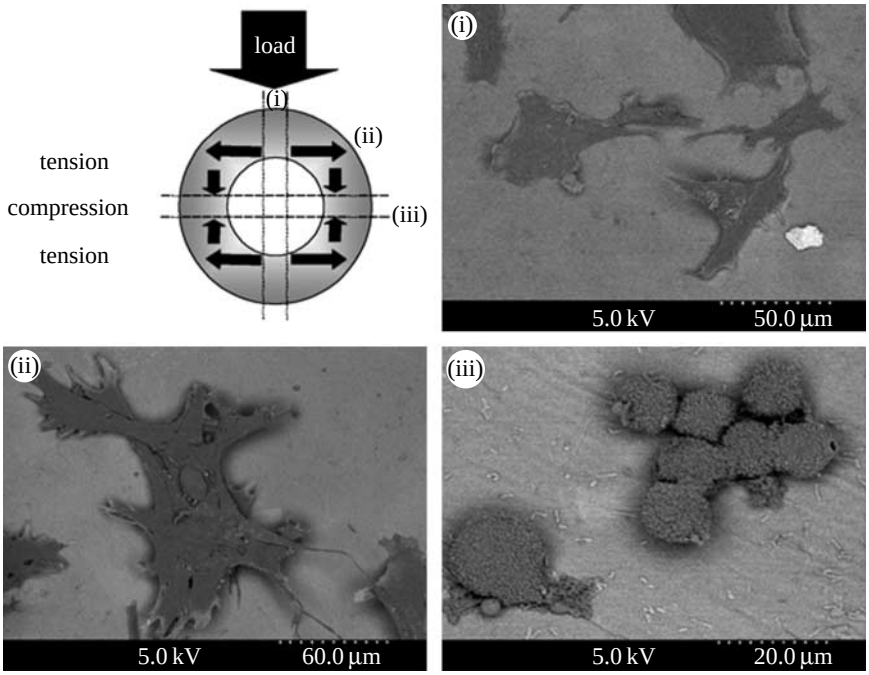

Figure 4. Schematic showing strain distribution in the single pore model during compression. (i–iii) Three areas within the tubing are highlighted. BSE imaging was used to determine bone cell morphology and medium- and high-density components relative to these regions.

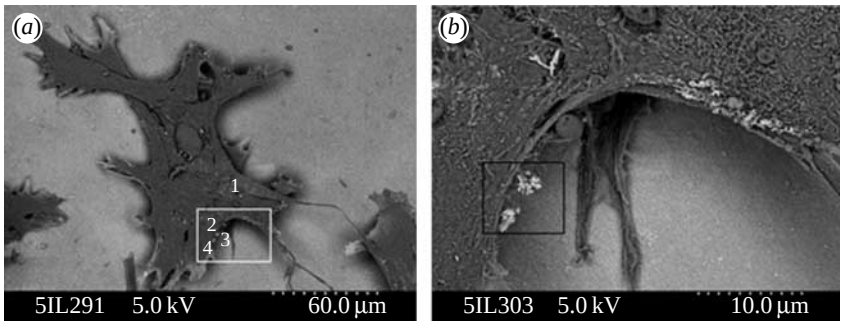

Figure 5. Low-magnification BSE imaging of bone cells using the Hitachi S-4100. (*a*) High-density features were identified as bright, contrasting entities, labelled 1–4. These sites were investigated using EDX as in figure 6. The white box highlights the area investigated at higher resolution (*b*). The black box in (*b*) highlights the area investigated at higher resolution as in figure 7.

portion of the mineral fraction (Vajda *et al.* 1998). However, calcium is used to identify the mineralized osteoid in the present study, limiting any inaccuracies regarding organic components.

3.5. Morphological identification of dense material using SE and BSE detection

High-magnification SE imaging indicated that the dense material observed using BSE imaging was coated with cellular material, possibly membrane (figure 7). BSE imaging of the high-density material (figure 7*b*) indicated that the calcium-containing entities are composed of agglomerates of rod- or needle-like structures.

3.6. Calcium distribution relative to strain profile

A series of zones were superimposed on a low-magnification BSE image of the pore model relative to the FE data (figure 8). Areas of maximum tension exhibit well-spread cells (similar to static controls), regions of maximum compression contain rounded or very few cells and regions of reduced surface strain, especially those closest to the area of maximum compression, display well-stretched multicellular agglomerates as previously demonstrated (figure 4). In figure 8, however, a zero-load zone has been included, as identified in the FE analysis, and contains few cells. The cells which are present within this region appear to have dislodged from the reduced strain region on the right, probably a result of sample handling, fixing and dehydration, as they bridge this zone and form connections with cells in the reduced strain region on the left. All zones were investigated at high magnification in BSE mode, but only dense entities were identified in cells and osteoid subjected to reduced surface strain relative to maximum tension and maximum compression sites. An area within each of these regions was investigated using BSE mode and six dense sites using EDX. The number of calcium agglomerates identified using this method were plotted

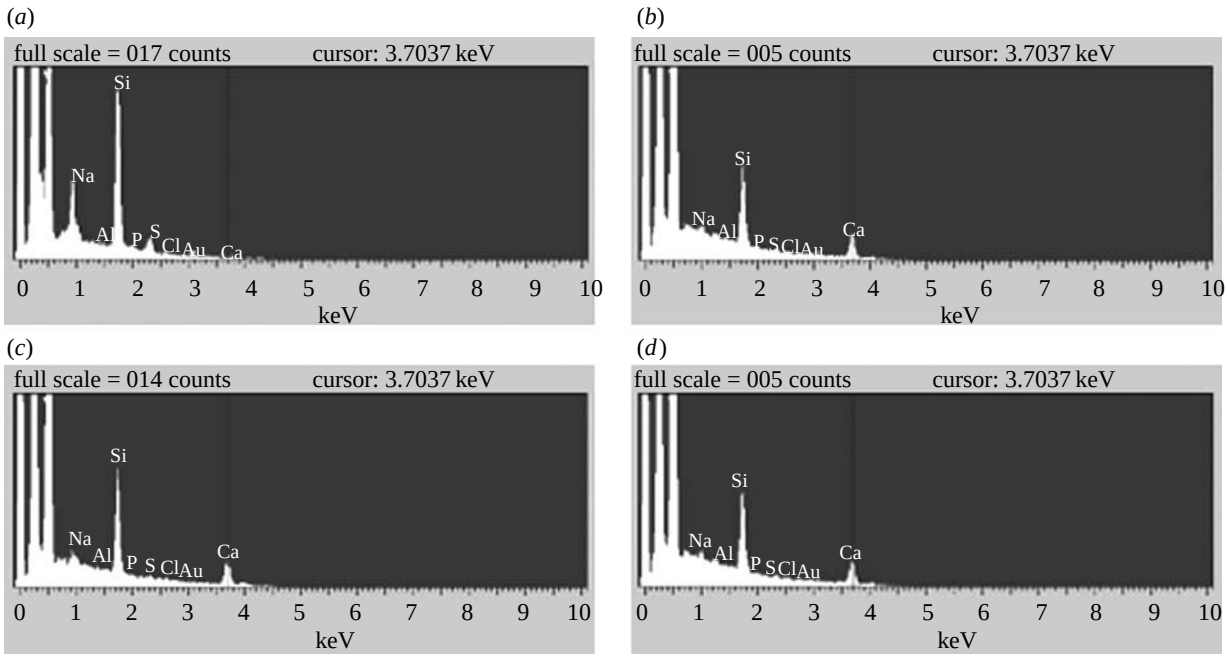

Figure 6. EDX spectra of points identified using BSE detection as in figure 5*a* and are labelled accordingly. (*a*) The first high-density entity identified (1), did not contain calcium, but was primarily composed of sodium and sulphur, spectrum 1. (*b–d*) The spectra 2–4 did contain calcium, highlighted with a cursor at 3.7 keV, thus these points were further investigated at higher resolution. The silicone peaks arise due to the silicone composition of the biomaterial upon which cells were cultured. The other peaks to the left of the spectra are background peaks including oxygen, nitrogen and carbon.

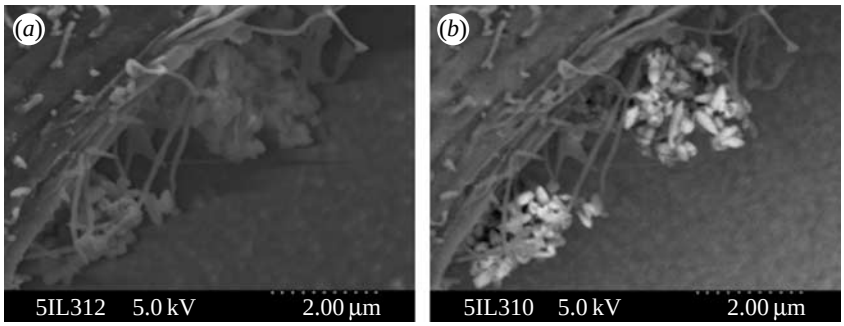

Figure 7. Higher resolution (*a*) SE and (*b*) BSE imaging of the calcium agglomerates identified in figure 5. SE imaging indicates that these crystal features underlie biological material, suggesting that they are of cellular origin. The interweaving filaments located around the crystals substantiate this. BSE imaging indicates that the calcium entities are composed of rod-like structures.

relative to local strain conditions, where data points are connected by lines suggesting a smooth transition between the amount of calcium produced as a result of strain in an ideal model (figure 9). These results indicate that two main sites of the pore model quadrant investigated, both of which are subjected to reduced surface strain, are capable of producing bone cell and osteoid mineralization under the experimental conditions outlined, namely 1% deformation of the tubing's outer diameter applied for 30 min d^{-1} for 3 days at 1 Hz in the presence of Bay K8644.

4. DISCUSSION

Through the use of our *in vitro* pore model, we have demonstrated that bone cell phenotype and differentiation is altered as a result of the strain profile. Bone cells experiencing different strains within the model, identified using FE analysis, exhibit distinctive morphologies. Specifically, cells subjected to compressive strains (up to 0.61%) appeared extremely rounded while those experiencing zero and tensile strain (up to 0.82%) exhibited flat and well-spread morphologies, similar to cells cultured under control static conditions. Only those cells exposed to a reduced level of strain with respect to regions of maximum tension and maximum compression form mineralized osteoid produced by multicellular aggregates. Mineralized tissue was absent from static controls and observed only in regions of our mechanically conditioned pore model where cells experienced reduced strain levels and formed multicellular aggregates with their neighbours, indicating the importance of cell–cell contacts for *in vitro* bone tissue production. Well-spread cells subjected to static conditioning in control samples and, in the mechanically conditioned single pore model maximum tension, rounded cells subjected to maximum compression and cells located within the 'zero-strain zone' are not inclined to produce mineralized matrix. These results indicate that alterations in bone cell morphology as a result of strain are paramount to osteoid

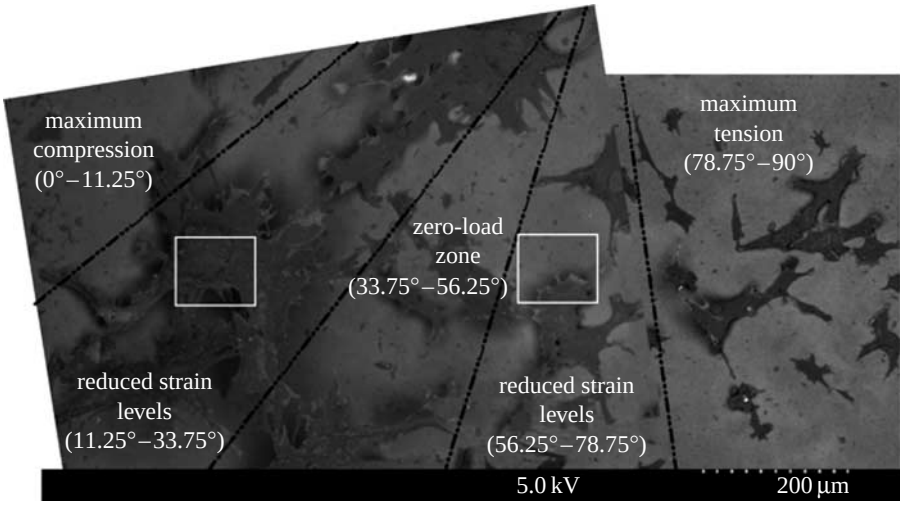

Figure 8. A visual representation of the zones determined in the FE analysis model. The image is composed of two BSE photomicrographs, which, combined, forms one quadrant of the pore model. The lines in the image are placed to help readers distinguish between each 'zone', also labelled in the image. The curvature of the tubing results in non-parallel zones. Strain angles relative to the FE model are stated for each zone. The boxes in the image highlight areas identified as containing calcium, deduced using BSE and EDX.

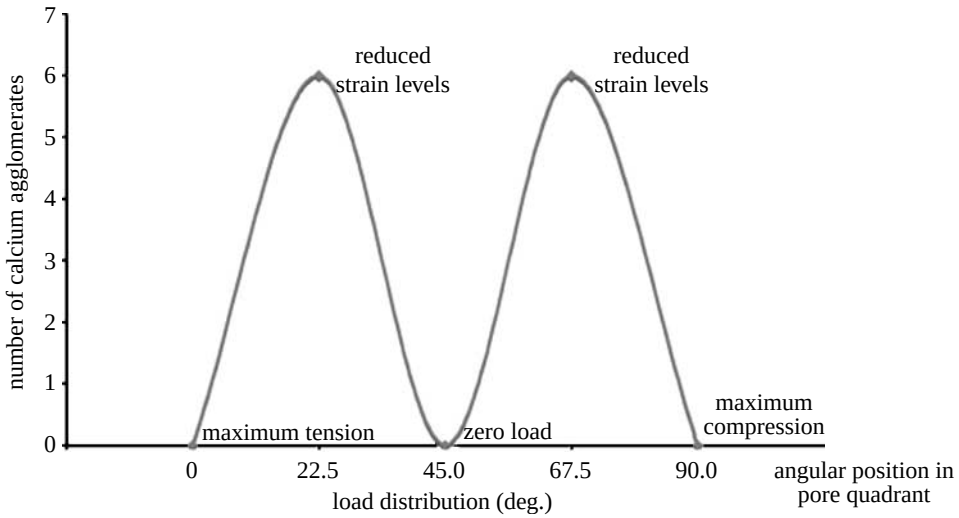

Figure 9. Calcium distribution relative to load within one quadrant of the pore model. A plot of the number of positively identified calcium agglomerates relative to local strain, highlighted in figure 8. Strain angles are included for reference. BSE mode was used to detect dense material relative to cells. Dense materials were observed only in areas subjected to reduced strain levels, on each side of the zero-load zone. An area within each zone was then investigated using EDX, where six agglomerates were investigated for their calcium content, all of which were positively identified.

mineralization. Cell–cell contacts appear to be fundamental with respect to the production of mineralized matrix occurring as a result of mechanical conditioning in the presence of the L-type VOCC-agonist Bay K8644. These findings suggest that the cell proliferation is not essential for bone tissue production *in vitro,* but rather cell–cell contacts are the driving force of bone formation, and can be induced using a stringent loading regime. It should be noted that static controls did not allow for cells to experience the shear forces of those in conditioned samples. However, the cells subjected to shear within the conditioned constructs at points of zero or low strain acted as a control for this situation.

The quantity and location of calcium in matrix vesicles or extracellular hydroxyapatite (HA) [$Ca_{10}(PO_4)_6(OH_2)$], the main component of bone mineral, are controlled by bone cells, supporting the importance of this element in identifying osteoid mineralization (Anderson 1995). When analysing the X-ray microanalysis data, a lack of phosphate, which would peak at approximately 1.9 keV on the graphs, was noted. This finding is of interest when considering the accuracy of EDX, which can detect an element composing only 1% of the volume under investigation, and previous suggestions that PO_4^{3-} accumulation is believed to precede that of calcium in relation to matrix vesicle mineralization (Anderson 1995). Our EDX analysis suggests that mechanical loading *in vitro* may potentially alter the process of mineralization identified with respect to matrix vesicles and osteoid *in vivo*.

Alterations in cell shape and adhesion are functionally and physically coupled to the genes by the tissue

matrix (Bidwell *et al.* 1998); thus alterations in cell morphology indicate alterations in cell behaviour and, ultimately, gene expression (Pavalko *et al.* 2003). The effects of bone cell morphology have previously been discussed, for example in the *ex vivo* formation of human bone subjected to cytokine treatments (Kale *et al.* 2000); yet little is documented concerning the effects of strain levels on bone cell morphology and osteoid mineralization *in vitro*, especially with respect to bone tissue engineering applications. Our model allows for the effects of load dissipation throughout a single pore to be deduced in relation to cell morphology and osteoid mineralization. Further development of this model may allow gene and protein expression to be investigated relative to strain profiles within a single pore of a more complex three-dimensional tissue-engineering scaffold, where strain levels are gauged using FE analysis. Identification of load-affected cell morphology and resultant differentiation allows for correlations to be identified with respect to cell shape, extracellular matrix production and mineralization, further enhancing our understanding of bone production. This information will enhance our understanding of tissue-engineered bone production *in vitro*, allowing for optimization of loading regimes in bioreactors and preconditioning of constructs.

The model outlined has been produced to provide insight into the distribution of strain occurring across individual pores within a complex porous tissue-engineering scaffold. It should be noted that a number of factors in our model have been simplified in relation to pores observed within scaffolds. For example, the size of pores within the scaffolds used for our bone tissue engineering applications range from 250 to 355 µm in diameter with a more complex, crystalline curvature occurring as a result of the salt leaching process (Wood *et al.* 2006*a*,*b*). These discrepancies must be taken into consideration when comparing the results of our model to three-dimensional porous scaffolds, and occur within our model to allow for more accurate image acquisition and precise location of strains relative to cells.

The single pore model provides a platform to enhance our understanding of the mechanisms employed by bone cells when sensing and responding to load and their ability to distinguish between strain types and strain magnitude. This information can be used to optimize tissue-engineered bone production in response to mechanical loading. Furthermore, this model offers an *in vitro* means of examining these factors in relation to the complex topological surface of bone (Pavalko *et al.* 2003), where the internal topography of pores can be altered through the application of fabrication techniques presently practiced (Wood *et al.* 2002; Berry *et al.* 2005; Wood 2007). Our model allows for variations in strain levels to be investigated, allowing for strain profiles similar to the heterogeneous distribution of load in trabecular bone (Niebur *et al.* 2000) to be examined in the presence of pharmacological or growth factors used in tissue engineering strategies and allowing for the development of enhanced bone tissue engineering protocols. This pore model may also provide a means of investigating bone injury response under controlled mechanical conditions *in vitro* and possible interventional strategies (Landry *et al.* 1996), and factors influencing the non-random event of matrix vesicle positioning (Anderson 1995) relative to load.

5. CONCLUSION

Our pore model provides a platform to enhance our understanding of the mechanisms employed by bone cells when sensing and responding to load *in vitro* and their ability to distinguish among strain types, strain direction and strain magnitude. Using FE analysis in conjunction with the model shows that cells express specific morphologies dependent upon localized strain profiles in the presence of Bay K8644. Those subjected to compressive strains (up to 1450 µstrain) appeared extremely rounded while cells experiencing zero and tensile strain (up to 1700 µstrain) exhibited flat and well-spread morphologies, similar to cells cultured under control static conditions. Only those cells exposed to a reduced level of strain with respect to regions of maximum tension and maximum compression form mineralized osteoid produced by multicellular aggregates, indicating the importance of cell–cell contacts for *in vitro* bone tissue production. Moreover, EDX analysis highlighted a lack of phosphate (present in HA, the main component of bone mineral) in mineralized tissue formed via mechanical loading *in vitro* suggesting that this process may potentially alter the process of mineralization identified with respect to matrix vesicles and osteoid *in vivo*. Thus the model offers an *in vitro* means of examining heterogeneous strains similar to those observed in trabecular bone to be examined in the presence of pharmacological or growth factors and in relation to the complex topological surface of bone allowing for the development of enhanced bone tissue engineering protocols. This pore model may also provide a means of investigating bone injury response under controlled mechanical conditions *in vitro* and possible interventional strategies, and factors influencing the non-random event of matrix vesicle positioning relative to load.

This work was funded by the EPSRC (GR/S11510/01) and AO Research Foundation. The authors would like to thank Christophe Sprecher for his technical support.

REFERENCES

Anderson, H. C. 1995 Section III regular and special features, molecular biology of matrix vesicles. *Clin. Orthop. Relat. Res.* **314**, 266–280.

Berry, C. C., Dalby, M. J., McCloy, D. & Affrossman, S. 2005 The fibroblast response to tubes exhibiting internal nanotopography. *Biomaterials* **24**, 4985–4992. (doi:10.1016/j.biomaterials.2005.01.046)

Bidwell, J. P., Alvarez, M., Feister, H., Onyia, J. & Hock, J. 1998 Nuclear matrix proteins and osteoblast gene expression. *J. Bone Miner. Res.* **13**, 155–167. (doi:10.1359/jbmr.1998.13.2.155)

El Haj, A. J., Wood, M. A., Thomas, P. & Yang, Y. 2005 Controlling cell biomechanics in orthopedic tissue engineering and repair. *Pathol. Biol. (Paris)* **53**, 581–589.

Hing, K. A. 2004 Bone repair in the twenty-first century: biology, chemistry or engineering? *Phil. Trans. R. Soc. A* **362**, 2821–2850. (doi:10.1098/rsta.2004.1466)

Ignatius, A., Blessing, H., Liedert, A., Schmidt, C., Neidlinger-Wilke, C., Kaspar, D., Friemert, B. & Claes, L. 2005 Tissue engineering of bone: effects of mechanical strain on osteoblastic cells in type I collagen matrices. *Biomaterials* **26**, 311–318. (doi:10.1016/j.biomaterials.2004.02.045)

Iqbal, J. & Zaidi, M. 2004 Molecular regulation of mechanotransduction. *Biochem. Biophys. Res. Commun.* **328**, 751–755. (doi:10.1016/j.bbrc.2004.12.087)

Kale, S., Biermann, S., Edwards, C., Tarnowski, C., Morris, M. & Long, M. W. 2000 Three-dimensional cellular development is essential for *ex vivo* formation of human bone. *Nat. Biotechnol.* **18**, 954–958. (doi:10.1038/79439)

Landry, P. S., Marino, A. A., Sadasivan, K. K. & Albright, J. A. 1996 Bone injury response: an animal model for testing theories of regulation. *Clin. Orthop. Relat. Res.* **332**, 260–273. (doi:10.1097/00003086-199611000-00034)

Mullender, M., El Haj, A. J., Yang, Y., van Duin, M. A., Burger, E. H. & Klein-Nulend, J. 2004 Mechanotransduction of bone cells *in vitro*: mechanobiology of bone tissue. *Med. Biol. Eng. Comput.* **42**, 14–21. (doi:10.1007/BF02351006)

Niebur, G. L., Feldstein, M. J., Yeun, J. C., Chen, T. J. & Keavney, T. M. 2000 High-resolution finite element models with tissue strength asymmetry accurately predict failure of trabecular bone. *J. Biomech.* **33**, 1575–1583. (doi:10.1016/S0021-9290(00)00149-4)

Nomura, S. & Takano-Yamamoto, T. 2000 Molecular events caused by mechanical stress in bone: mini review. *Matrix Biol.* **19**, 91–96. (doi:10.1016/S0945-053X(00)00050-0)

Oakes, B. W. 2004 Orthopaedic tissue engineering: from laboratory to the clinic. *MJA Suppl.* **180**, S35–S38.

Palluel, P. 1947 Diffusion composition of secondary electron rays in metals. *Compt. Rend. Acad. Sci. (Paris)* **224**, 1492–1494.

Pavalko, F. M., Norvell, S. M., Burr, D. B., Turner, C. H., Duncan, R. L. & Bidwell, J. P. 2003 A model for mechanotransduction in bone cells: the load-bearing mechanosomes. *J. Cell Biochem.* **88**, 104–112. (doi:10.1002/jcb.10284)

Salgado, A. J., Coutinho, O. P. & Reis, R. L. 2004 Bone tissue engineering: state of the art and future trends. *Macromol. Biosci.* **4**, 743–765. (doi:10.1002/mabi.200400026)

Sikavitsas, V. I., Temenoff, J. S. & Mikos, A. G. 2001 Biomaterials and bone mechanotransduction: review. *Biomaterials* **22**, 2581–2593. (doi:10.1016/S0142-9612(01)00002-3)

Turner, C. H. & Robling, A. G. 2004 Exercise as an anabolic stimulus for bone. *Curr. Pharm. Des.* **10**, 2629–2641. (doi:10.2174/1381612043383755)

Vajda, E. G., Bloebaum, R. D. & Skedros, J. G. 1996 Validation of energy dispersive X-ray spectrometry as a method to calibrate backscattered electron images of bone. *Cells Mater.* **6**, 79–92.

Vajda, E. G., Skedros, J. G. & Bloebaum, R. D. 1998 Errors in quantitative backscattered electron analysis of bone standardized by energy-dispersive X-ray spectrometry. *Scanning* **20**, 527–535.

Walker, L. M., Publicover, S. J., Preston, M. R., Said Ahmed, M. A. A. & El Haj, A. J. 2000 Calcium-channel activation and matrix protein upregulation in bone cells in response to mechanical strain. *J. Cell. Biochem.* **79**, 648–661. (doi:10.1002/1097-4644(20001215)79:4<648::AID-JCB130>3.0.CO;2-Q)

Wood, M. A. 2007 Review: colloidal lithography and current fabrication techniques producing in-plane nanotopography for biological applications. *J. R. Soc. Interface* **4**, 1–17. (doi:10.1098/rsif.2006.0149)

Wood, M. A., Meredith, D. O. & Owen, G. Rh. 2002 Steps towards a model nanotopography. *IEEE Trans. Nanobiosci.* **1**, 133–140. (doi:10.1109/TNB.2003.809460)

Wood, M. A., Meredith, D. O., Owen, G. Rh., Richards, R. G. & Riehle, M. O. 2005 Utilising atomic number contrast for FESEM imaging of colloidal nanotopography underlying biological cells. *Nanotechnology* **16**, 1433–1439. (doi:10.1088/0957-4484/16/9/002)

Wood, M. A., Hughes, S., Yang, Y. & El Haj, A. J. 2006*a* Characterizing the efficacy of calcium channel agonist-release strategies for bone tissue engineering applications. *J. Control Release* **112**, 96–102. (doi:10.1016/j.jconrel.2006.01.008)

Wood, M. A., Yang, Y. & El Haj, A. J. 2006*b* Using dihydropyridine-release strategies to enhance load effects in engineered human bone constructs. *Tissue Eng.* **12**, 2489–2497. (doi:10.1089/ten.2006.12.2489)

Yang, Y., Magnay, J. L., Cooling, L. & El Haj, A. J. 2002 Development of a 'mechano-active' scaffold for tissue engineering. *Biomaterials* **23**, 2119–2126. (doi:10.1016/S0142-9612(01)00342-8)